www.advopticalmat.de

ADVANCED OPTICAL MATERIALS

RESEARCH ARTICLE

Unidirectional Focusing of Light Using Structured Diffractive Surfaces

*Yuhang Li, Tianyi Gan, Jingxi Li, Mona Jarrahi, and Aydogan Ozcan**

Unidirectional optical systems enable selective control of light through asymmetric processing of radiation, effectively transmitting light in one direction while blocking unwanted propagation in the opposite direction. Here, a reciprocal diffractive unidirectional focusing design based on linear and isotropic diffractive layers that are structured is introduced. Using gradient descentbased optimization, a cascaded set of diffractive layers are spatially engineered at the wavelength scale to focus light efficiently in the forward direction while blocking it in the opposite direction. The forward energy focusing efficiency and the backward energy suppression capabilities of this unidirectional architecture are demonstrated under various illumination angles and wavelengths, illustrating the versatility of the polarization-insensitive design. Furthermore, it is demonstrated that these designs are resilient to adversarial attacks that utilize wavefront engineering from outside. Experimental validation using terahertz radiation confirmed the feasibility of this diffractive unidirectional focusing framework. Diffractive unidirectional designs can operate across different parts of the electromagnetic spectrum by scaling the resulting diffractive features proportional to the wavelength of light and will find applications in security, defense, and optical communication, among others.

1. Introduction

The control of asymmetric light propagation, where light preferentially travels in one direction while being suppressed or scattered in the opposite direction, has enabled various advancements in optical systems. Achieving such directional control of light propagation is crucial for applications in wave transmission, imaging, and sensing.[1–3] However, most optical systems based on linear and time-invariant components are inherently bidirectional. Breaking this to enable asymmetric light propagation presents some challenges. Traditional approaches often rely on advanced material properties, such as the magnetooptic effect[4–7] or nonlinear materials.[8–10] These methods, while effective, are typically associated with relatively bulky and costly setups due to their tight fabrication requirements and rely on high-power laser sources to introduce sufficient nonlinearity. Additionally, asymmetric isotropic dielectric gratings[11–13] and metamaterials[14–18] have been explored to create unidirectional material systems. Although these approaches demonstrated success, such systems are often limited in scope due to their complex design and fabrication processes, polarization sensitivity, and poor performance under off-axis illumination.

In this work, we report a reciprocal diffractive optical system designed for unidirectional focusing of radiation, where the incoming light is focused in the forward direction while being blocked or scattered in the opposite direction, as illustrated in **Figure 1**. This unidirectional propagation is achieved using structurally optimized linear and isotropic diffractive layers with wavelength-scale features that are optimized using gradient descent. The unidirectional system's energy-blocking capability in the backward direction was evaluated under multi-angle illumination. Incorporating various illumination angles during the optimization process enhanced the system's light-blocking performance in the backward direction, enabling it to generalize effectively across different angles of illumination. Furthermore, this training strategy also improved the unidirectional system's resilience against adversarial attacks, making it impractical to focus light in the backward direction regardless of wavefront engineering from outside. Additionally, we extended our polarizationinsensitive unidirectional focusing designs to operate across multiple wavelengths, demonstrating the ability to maintain unidirectional light control within a broad spectral range of interest. The proof of concept of this unidirectional focusing framework was

Y. Li, T. Gan, J. Li, M. Jarrahi, A. Ozcan
Electrical and Computer Engineering Department
University of California
Los Angeles, CA 90095, USA E-mail:
ozcan@ucla.edu
Y.Li,T.Gan,J.Li,M.Jarrahi,A.Ozcan
CaliforniaNanoSystemsInstitute(CNSI)
UniversityofCalifornia
LosAngeles,CA90095,USA
A.Ozcan
BioengineeringDepartment UniversityofCalifornia
LosAngeles,CA90095,USA

The ORCID identification number(s) for the author(s) of this article can be found under https://doi.org/10.1002/adom.202403371

DOI: 10.1002/adom.202403371
Adv. Optical Mater. **2025**, *13*, 2403371

experimentally validated using 3D-printed diffractive layers that operate at the terahertz part of the spectrum. We believe that

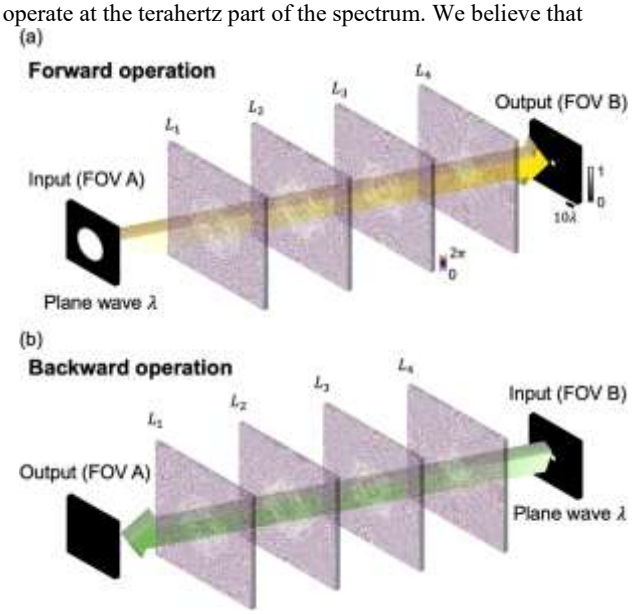

Figure 1. Schematic of unidirectional focusing using a diffractive processor. a) The diffractive system focuses light efficiently in the forward direction (A → B). b) The system blocks and scatters light in the backward direction (B → A).

the presented diffractive unidirectional focusing architecture will findvariousapplicationsindefense/security,opticalcommunication, imaging, and sensing.

2. Result

2.1. Unidirectional Focusing of Light Using Structured Diffractive Materials

Our framework for unidirectional focusing of coherent light is illustrated in Figure 1. Light entering the system through an input aperture, i.e., the input field of view A (FOV A), is focused onto a specific output region/aperture within FOV B (A → B defining the forward focusing operation, Figure 1a), whereas the light originating from the aperture in FOV B is scattered out (B → A defining the backward operation, Figure 1b). As shown in **Figure 2**a, the unidirectional focusing design consisted of four phase-only diffractive layers, each containing 240 × 240 phasemodulating features, ˜⍰/2 in lateral size, where ⍰ is the illuminationwavelength.Thephasemodulationofeachdiffractivefeature ranges from 0 to 2⍰, achieved by adjusting its local thickness (refer to the Experimental Section for details). The diffractive layers are surrounded by opaque regions that block light. These regions prevent light from bypassing the diffractive structures, ensuring distinct transmission characteristics for the forward and backward operations, thus contributing to the unidirectional lightfocusing performance.

During the design optimization process, the phase values of the diffractive layers were iteratively updated using a stochastic gradient descent-based algorithm and a custom loss function. This loss function was mathematically constructed to maximize the output energy efficiency in the forward path (A → B) while minimizing the energy efficiency in the backward path (B

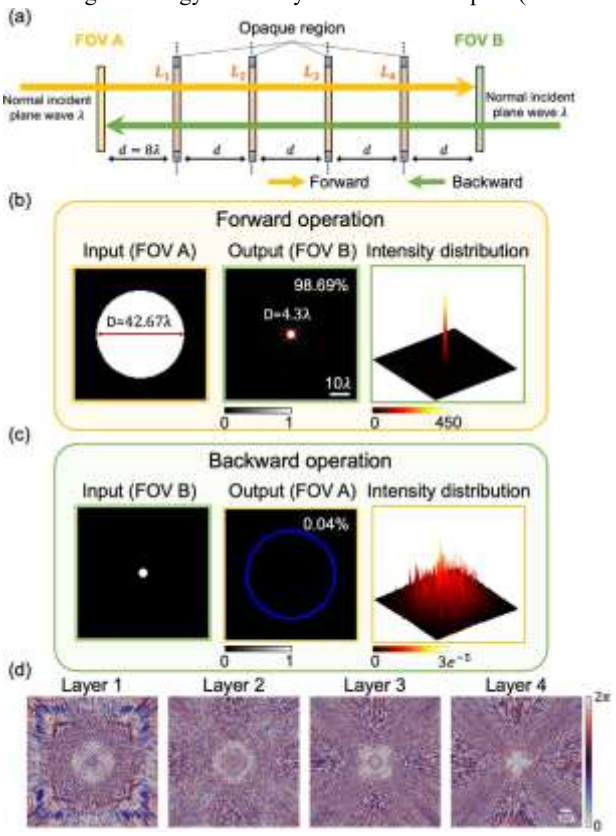

Figure 2. Design schematics and numerical results of the diffractive unidirectional focusing system. a) Schematic layout of a four-layer unidirectional focusing system for normal incidence plane wave. The diffractive layers are surrounded by opaque regions that block light. b) Forwarddirection light focusing performance (A → B). c) Backward-direction light blocking performance (B → A). d) Phase profiles of the trained diffractive layers.

→ A). After its training, the system can successfully focus a plane wave passing through an aperture in FOV A into a tightly focused spot at the output (FOV B) within a diameter of 4.3⍰, while effectively blocking the light traveling in the reverse direction, B → A. As shown in Figure 2b,c, the forwardfocusing operation achieved ˜98.7% energy efficiency within the target output region (FOV B), whereas the backward illumination resulted in only ˜0.4% energy detected in FOV A.

Thephasemodulationpatternsoftheoptimizeddiffractivelayers are visualized in Figure 2d. One can observe that the diffractive layers exhibit an asymmetric structure from A to B versus B to A, and the central regions of the resulting diffractive layers exhibit lens-like structures, which are crucial for the efficient focusing of light in the forward operation. However, the edge regions of each diffractive layer adopt grating-like structures that scatter and diffuse light

during the backward operation, enhancing beam suppression in the reverse illumination path.

These numerical analyses underscore the effectiveness of phase-only diffractive designs in achieving efficient unidirectional focusing of light through structural asymmetry. By leveraging customized loss functions and gradient descentbased optimization, this approach enables diffractive systems to selectively control light propagation properties in different directions. We also visualized the evolution of the optical fields propagating within this unidirectional focusing design, as shown in Figure S1 (Supporting Information). During the forward operation, the light was noticeably focused after passing through the L_3 and L_4 layers. In contrast, during the backward operation, significant losses occur after the L_2 and L_1 layers. We also used the output optical field resulting from the forward operation as the input field for the backward operation, simulating a reflection scenario at the output plane. As shown in Figure S2a,b (Supporting Information), the energy transmission efficiency detected in FOV A was ˜66.8% when the output optical field resulting from the forward operation was used as the input field for the backward operation. Despite being a reciprocal system, the backward transmission in this case does not reach 100% because the system does not obey time-reversal symmetry due to the lossy regions surrounding the diffractive layers. Furthermore, as shown in Figure S2c (Supporting Information), when only the amplitude profile of the output optical field resulting from the forward operation was used as the input for the backward operation, with a flat phase profile, the backward energy transmission dropped to 11.49%. To further reduce this backward reflection-related leakage, we trained an alternative unidirectional focusing system using the forward operation's output field as the input for the backward operation during the training stage (see the Experimental Section for details). As illustrated in Figure S3 (Supporting Information), the resulting design demonstrates that the forwardfocusing operation achieved ˜98.2% energy transmission efficiency within the target output region (FOV B), while the backward operation using the output optical field resulting from the forward operation led to only ˜5% backward energy transmission detected in FOV A; also see Figure S4 (Supporting Information) for additional unidirectional focusing systems designed with the same strategy. These results provide additional insights into the operation mechanisms of unidirectional focusing systems. Further analyses on the distribution of various loss factors within the diffractive device volume will be provided in the following sections.

2.2. Robustness of Diffractive Focusing Systems Under Oblique Illumination and Adversarial Attacks

While our diffractive focusing system reported in Figure 2 exhibits a very good unidirectional performance under normal illumination, real-world scenarios often involve oblique incidences of incoming radiation. To evaluate the robustness of our design, we analyzed its behavior under oblique illumination. Specifically, we tested the backward operation (B → A) of the system in Figure 2 using plane waves incident at various illumination angles relative to the optical axis, as shown in **Figure 3**a. The phase distributions were adjusted to control the incidence angle, maintaining uniform amplitude within the aperture of FOV B. Initially, the system was trained exclusively with plane waves propagating normally to the input aperture. While this approach effectively blocked the reverse beam propagation (B → A) for the normal incidence of illumination, its performance deteriorated as the incidence angle increased in the testing phase. For illumination angles approaching ˜20°, the suppression capability of

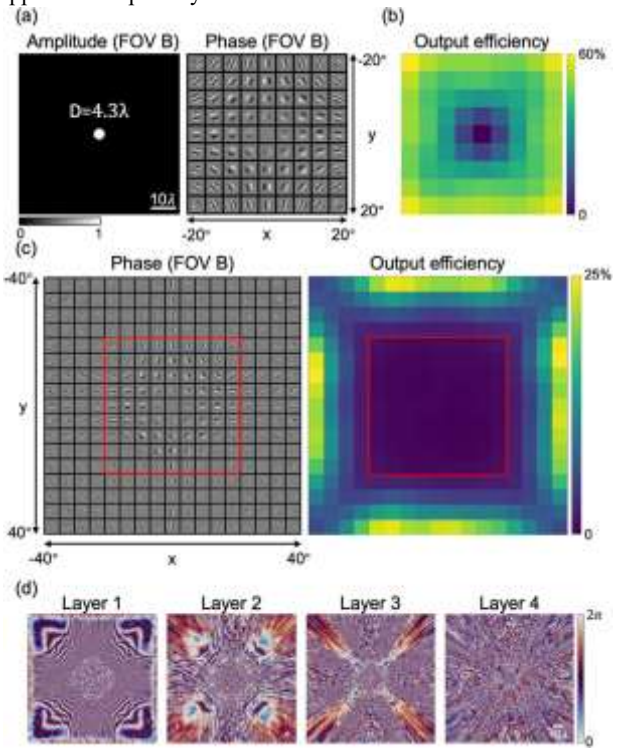

Figure 3. Light-blocking performance under oblique illumination. a) Input amplitude and phase patterns corresponding to illumination at various incidence angles at FOV B in the backward operation. b) Output energy efficiency values of the unidirectional focusing system (trained with normal incidence angle only) under different incidence angles, showing performance degradation under oblique illumination. c) Phase profiles and corresponding output energy efficiency values in the backward direction for the system tested under different incidence angles; the red box indicates the range of the incidence angles included during the training stage. This system showed improvements in suppressing the backward beam over a wide range of angles, even for those beyond the training range. d) Phase profiles of the diffractive layers trained with multi-angle illumination.

the diffractive system for B → A significantly degraded, allowing as much as 60% of the energy to leak into FOV A in the backward direction (see Figure 3b).

To address this performance limitation under oblique illumination, we implemented a multi-angle training strategy that incorporated diverse illumination conditions during the optimization of the cascaded diffractive layers. Forward operation (A → B) training remained limited to normal incidence, but the backward operation (B → A) was trained using various oblique waves randomly selected within a specified illumination range

[θ_{min}, θ_{max}]. The same loss function described in the Experimental section, under the "Training Loss Function and Evaluation Metrics" subsection, was used to penalize all the illumination angles in the backward operation. This approach allowed the diffractive system to generalize its beam suppression response in the backward direction across a broad range of oblique illumination angles by optimizing the phase modulation patterns of the diffractive layers. As shown in Figure 3c, this multi-angle-trained system demonstrated substantial performance improvements. During its training, [θ_{min},θ_{max}] was selected as [− 20°, 20°] (red box in Figure 3c), while the blind testing of its performance was conducted over a broader range of illumination angles covering [− 40°, 40°]. Compared to the original diffractive system trained only for the normal incidence of illumination, the multi-angle-trained diffractive unidirectional system showed significant improvements in its backward beam suppression capability across a wide range of angles, with only a minor reduction in the forward beam focusing efficiency, dropping to 97.2% from ˜98.7% of the previous design. Notably, even for the incident angles beyond the training range, the diffractive unidirectional system maintained a good beam suppression capability in the reverse direction. In this improved design, the trained diffractive layers, shown in Figure 3d, featured more complex patterns, particularly around the edge regions, which contribute to enhanced optical scattering and losses during the backward operation with oblique illumination angles.

Another critical consideration is the potential vulnerability of the unidirectional beam-focusing system to *adversarial* manipulations from the outside. For example, if an adversary from outside has access to the optical signal at FOV A through a "spying" detector, they could optimize the structure of the incident phase at FOV B by manipulating the wavefront in the backward direction (B → A) to gradually increase the energy at the output FOV A. To assess this vulnerability from the outside, we performed phase optimization on the incident wave in the backward path using iterative feedback from the optical signal observed at FOV A (see the Experimental Section for details). As shown in **Figure 4**a, diffractive unidirectional systems trained exclusively with the normal incidence of illumination were highly susceptible to such adversarial attacks, with the energy leakage in the backward direction reaching ˜88% through feedback-based learning using a "spying" detector at FOV A. This high energy leakage under an optimized attack underscores the limited robustness of these systemstoadversarialphasemanipulationfromoutside.Incontrast, themulti-angle-traineddiffractiveunidirectionalsystemreported in Figure 3 exhibited much better resilience to such adversarial attacks. By optimizing the phase modulation patterns for a range of incidence angles, the diffractive layers exhibited more complex and resilient structures, making it much harder for an adversary to find an optimal phase configuration to "hack" the system in the reverse path, B → A. Consequently, the resulting energy efficiency in the backward path was significantly lower than it was in the vanilla diffractive unidirectional systems. This increased robustness against adversarial attacks from outside underscores the advantages of training diffractive unidirectional systems with diverse illumination conditions, enhancing not only their generalization capabilities but also their resilience to targeted attacks from outside.

Expanding the training process to include an even wider range of illumination angles and other wavefront perturbations can ensure stronger energy suppression in the backward path, even under challenging or adversarial conditions. Such strategies are critical for developing practical and reliable diffractive unidirectional focusing systems for real-world applications.

Finally, we should emphasize that in the adversarial attacks that were considered here, we assumed that there was direct access to the beam power at FOV A in order to iteratively optimize the attacking wavefront in the reverse direction; without such an internal feedback mechanism through, e.g., a "spy" from inside, an adversary from outside alone would not be able to find practical and easy-to-implement methods to send

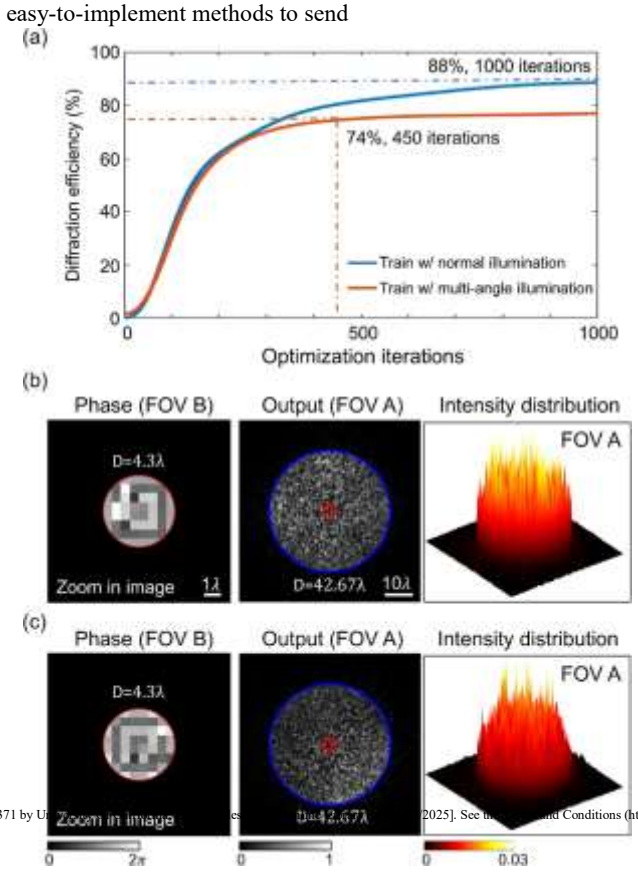

Figure 4. Adversarial attacks on the unidirectional focusing system. a) An iterative adversarial attack on the unidirectional diffractive system is performed from outside using a "spy" detector from inside. Optimization iterations of phase patterns in FOV B versus the leakage energy efficiency in the backward direction. b) Converged phase profiles in FOV B, output intensity in the backward direction (B → A), and the resulting intensity distribution at FOV A for the system trained only with normal incidence angle in the backward operation. c) Corresponding results for the diffractive unidirectional system trained with multiple incidence angles in the backward operation. These adversarial attacks utilized direct access to the beam power at FOV A for iteratively optimizing the attacking wavefront profile from outside. Without this internal feedback using a spying detector at FOV A, such an adversarial attack cannot be successful from outside.

radiation in the backward direction unless the design of the diffractive unidirectional material and its layers are a priori known.

2.3. Multi-Wavelength Operation

We further demonstrate that the diffractive focusing framework can operate at multiple illumination wavelengths, as shown in **Figure 5**a. The system, configured similarly to the previously shown monochromatic unidirectional design, was trained using three illumination wavelengths: 0.7, 0.75, and 0.8 mm. After its training, the diffractive unidirectional focusing design achieved forward focusing efficiencies of 92.42%, 93.46%, and 91.69% for the three illumination wavelengths, respectively. In the backward operation, the system effectively blocked the input light, with a leakage of 2.79%, 1.36%, and 1.71% at these 3

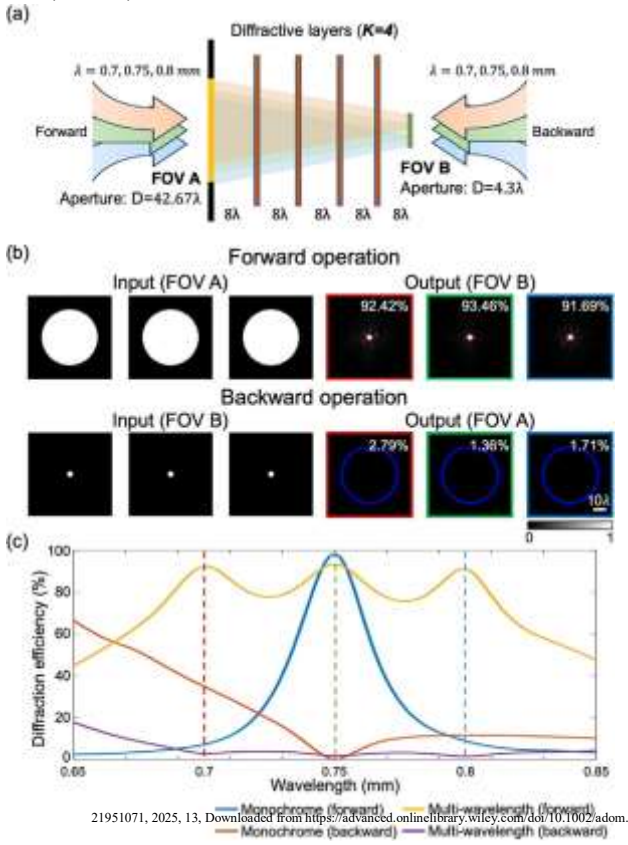

Figure 5. Multi-wavelength unidirectional focusing systems and their spectral responses. a) Schematic representation of the multi-wavelength unidirectional focusing system, designed to achieve unidirectional focusing at three distinct wavelengths. b) Input and output intensity profiles for the forward (A → B) and backward (B → A) directions at three illumination wavelengths under normal incidence plane wave illumination. The system demonstrates efficient forward beam focusing while significantly blocking backward propagation across all three wavelengths. c) Spectral responses of the diffractive unidirectional focusing system trained with monochrome illumination compared to its counterpart trained with multi-wavelength illumination. The multi-wavelength-trained system shows improved spectral performance across a broader range of wavelengths.

wavelengths, 0.7, 0.75, and 0.8 mm, respectively. However, this multi-wavelength operation comes with a slight performance trade-off. Compared to the monochromatic unidirectional design, the multi-wavelength system exhibited a small reduction in the peak forward diffraction efficiency. For a given number of trainable diffractive degrees of freedom, this behavior reflects the inherent balance between optimization of the unidirectional focusing performance for a specific wavelength versus achieving broader spectral functionality. These reported multiwavelength performance metrics can be further improved using deeperdiffractivedesignswithmoredegreesoffreedomavailable for optimization.

We also blindly evaluated the performance of the diffractive unidirectionalfocusingsystemunderilluminationacrossarange of wavelengths. For the system trained with monochromatic illumination at □ = 0.75 mm, the unidirectional focusing performance degraded significantly as the wavelength deviated from the training wavelength, as shown with the blue and red lines in Figure 5c. In the forward direction (A → B), the diffraction efficiency dropped sharply outside the optimal spectral range that the diffractive system was trained for. Similarly, in the backward operation (B → A), the energy leakage percentage increased, particularly for wavelengths shorter than 0.75 mm.

In contrast, the diffractive unidirectional focusing design trained with three distinct wavelengths (0.7, 0.75, and 0.8 mm) demonstrated far superior spectral performance. It maintained over >70% forward focusing efficiency across a broader spectral range while suppressing the backward illumination to <5% from 0.690 to 0.814 mm illumination. As indicated by the yellow and purple lines in Figure 5c, the multi-wavelength training significantly improved the system's output efficiency for wavelengths not explicitly used during the training—which indicates the *external generalization* behavior of the diffractive unidirectional processor outside of its training spectral range.

We further analyzed the power distribution of different modes within the diffractive volume for both the monochrome and multi-wavelength designs during the forward and backward operations, as shown in **Figure 6**. In the forward path (A → B), the majority of the input power is effectively focused within the target region (as desired), while the optical modes outside FOV B and the unbound modes remain minimal. Conversely, in the backward path (B → A), most of the input power escapes the diffractive volume through unbounded modes (green), illustrating the system's capability to suppress backward transmission and enhance unidirectional focusing behavior.

2.4. Experimental Demonstration of a Diffractive Unidirectional Focusing System

We experimentally validated our diffractive unidirectional focusing design using monochromatic continuous-wave terahertz illumination at □= 0.75 mm, as shown in **Figure 7**. The schematic diagram of the terahertz setup is presented in Figure 7a, with implementation details reported in the Experimental Section. For this experimental validation, we designed a diffractive unidirectional focusing system consisting of two diffractive layers, each composed of 120 × 120 learnable diffractive features, each with a lateral size of 0.64 □. The axial spacing between the adjacent planes was set to ˜26.7 □. The aperture size of FOV A was 42.67□,

while the aperture of FOV B was 6.4 □ (at the output focus plane). Unlike previous designs that assumed phase-only diffractive layers, this model incorporated the complex-valued refractive index of the 3D-printing diffractive material to account for material absorption, ensuring that optical absorption by the layers was mathematically taken into account during the gradient descent-based design process.

After the optimization phase, the resulting diffractive layers were fabricated using 3D printing, as shown in Figure 7c. The experimental performance of the fabricated system was evaluated for both the forward and the backward operations, as depicted in Figure 7d. This monochrome diffractive design (trained for operation at □ = 0.75 mm) was tested using five different wavelengths: {0.7, 0.725, 0.75, 0.775, 0.8} mm. Experimental performance of the diffractive system was quantitatively assessed at different illumination wavelengths using a signal-to-noise ratio (SNR) metric (see the Experimental Section for details). The results demonstrated that the 3D-printed diffractive unidirectional focusing system successfully focused light within the target output region in the forward direction (A → B) while effectively suppressing light in the backward direction (B → A) across the tested wavelength range. Notably, despite being trained only at an illumination wavelength of 0.75 mm, the 3D-printed diffractive design exhibited robust performance within a relatively large spectral range (±6.67% of the central design wavelength), showcasing its ability to handle illumination wavelength deviation from the training. These results demonstrate the experimental feasibility and spectral adaptability of the presented diffractive unidirectional focusing framework.

While the experimental results align well with their numerical counterparts in terms of general unidirectional beam-focusing performance, some discrepancies between the two were also observed. These differences can be attributed to several factors,

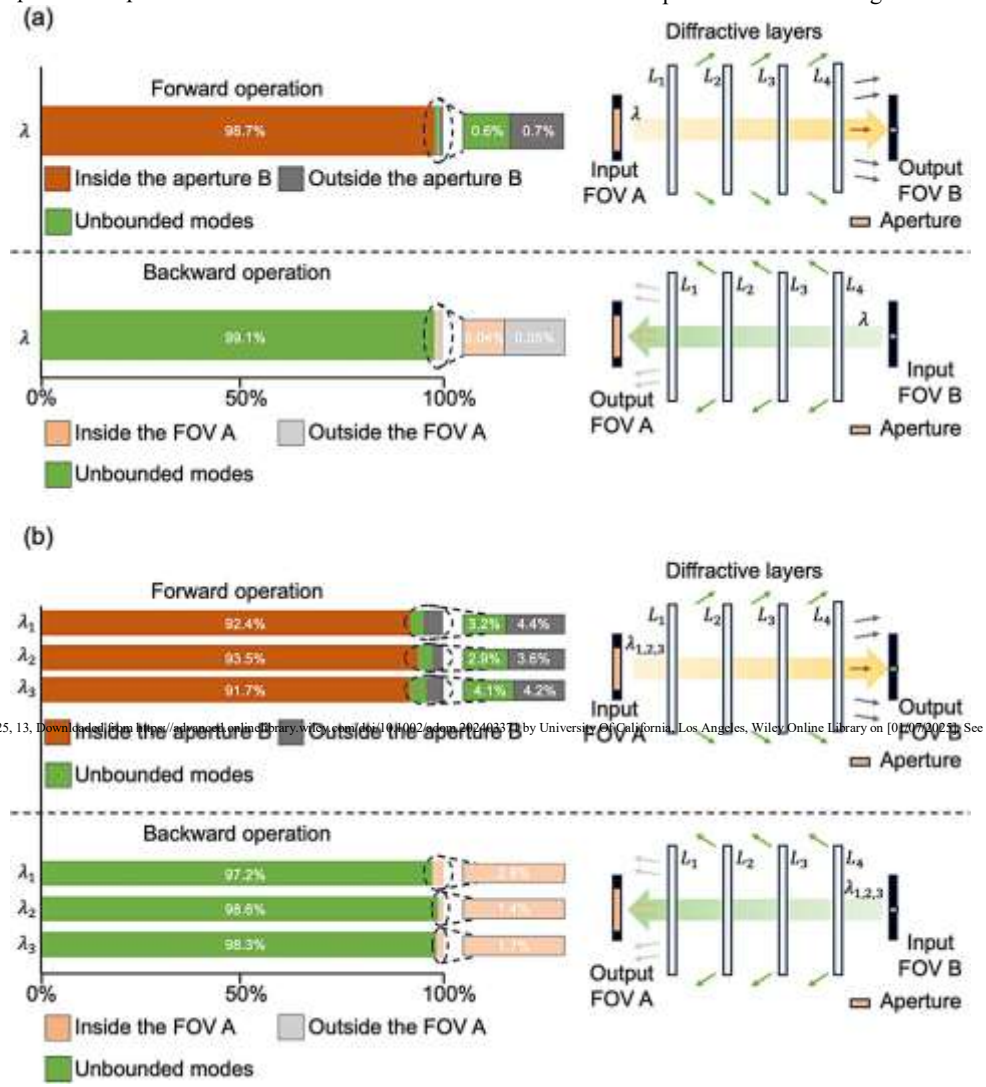

Figure 6. Performance analysis of unidirectional focusing systems. Left: The power distribution across different spatial modes for a) the monochrome and b) the multi-wavelength unidirectional focusing systems during the forward and backward operations. For the backward operation in the multiwavelength design, the energy outside FOV A is negligible (<0.01%), and, therefore, is not shown in the chart. Right: A schematic representation of the propagation of different spatial modes within the diffractive volume.

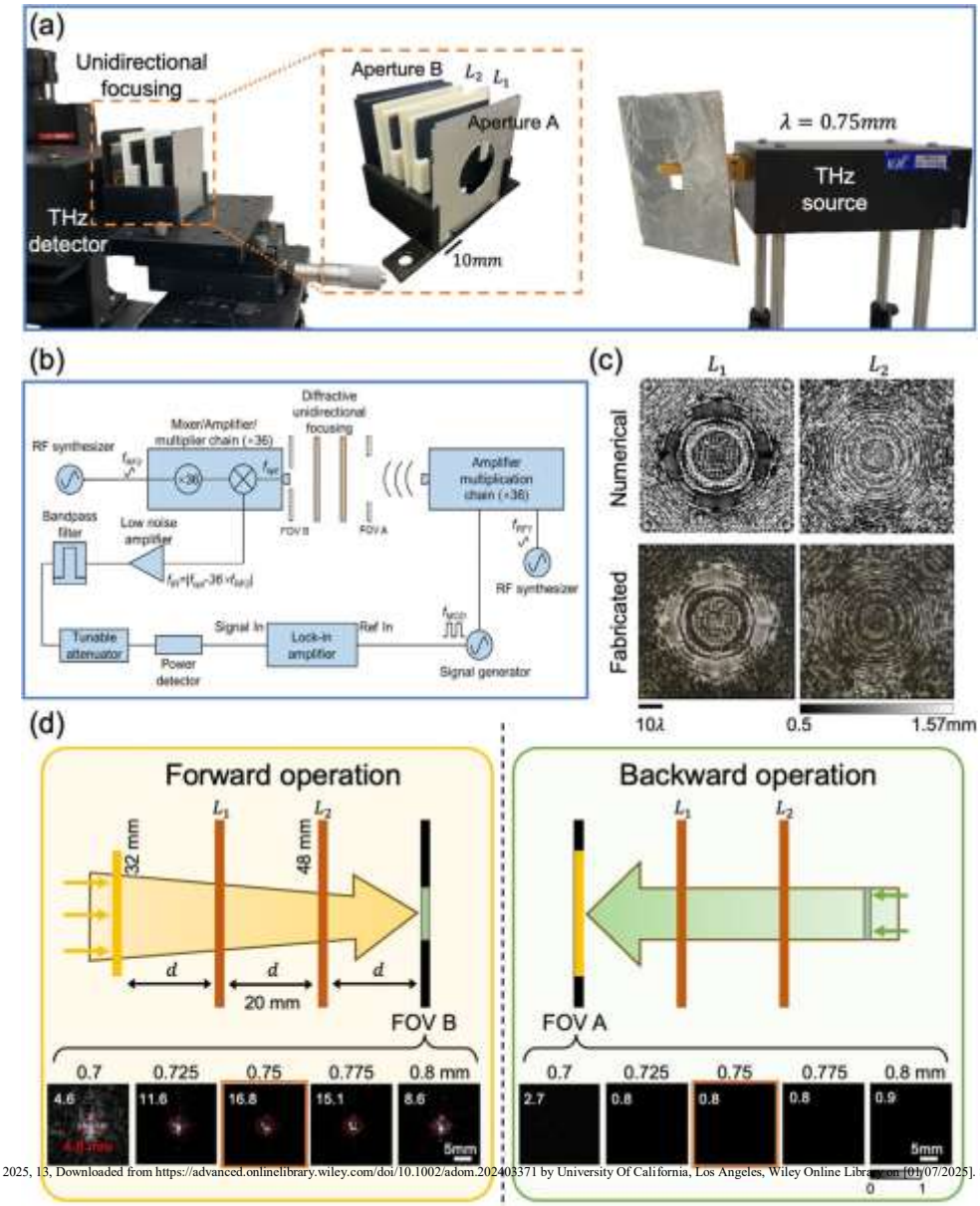

Figure 7. Experimental setup and results for the diffractive unidirectional focusing system. a) Photograph of the experimental setup, including the fabricated diffractive system. b) Schematic diagram of the continuous-wave terahertz setup. c) Phase patterns of the learned diffractive layers alongside the photographs of the 3D-printed diffractive layers. d) Experimental results for the forward beam focusing and backward beam blocking for five different illumination wavelengths {0.7, 0.725, 0.75, 0.775, 0.8} mm. The system was trained at a central wavelength of 0.75 mm (highlighted with an orange box). SNR values for each illumination wavelength are provided in the top-left corner.

including material losses, fabrication errors, and alignment challenges in the experimental setup. Material losses and absorption in the 3D-printed diffractive layers can result in reduced efficiency compared to the ideal numerical simulations. Additionally, fabrication errors, such as deviations in the layer thickness or surface roughness that might result during the 3D printing stage, could introduce phase inaccuracies that affect the system's performance. Furthermore, physical misalignments in the experimental setup, including relative positioning errors between the diffractive layers and the detector plane, may contribute to additional performance discrepancies between our numerical and experimental results.

3. Discussion

In this work, we introduced a diffractive unidirectional focusing framework, showcasing the potential of all-optical diffractive processors for asymmetric light manipulation. The system demonstrated efficient forward light focusing while effectively suppressing energy leakage in the backward direction. By incorporating multi-angle illumination during the training, the system's robustness was enhanced, allowing it to maintain unidirectional performance under oblique random illumination.

This diverse training approach also improved its generalization capabilities, mitigating energy leakage from oblique incident waves in the backward direction, and further increased resilience against adversarial attacks from outside. Additionally, we explored the unidirectional system's spectral response and broadband performance, showcasing the effectiveness of involving multiple wavelengths during the training phase to adapt the system to work under a broader illumination spectrum. Moreover, the feasibility of this unidirectional focusing framework was validated experimentally using monochromatic terahertz illumination, confirming its practical implementation.

It is important to distinguish our diffractive unidirectional focusing system from a traditional optical isolator. Optical isolators achieve nonreciprocal light transmission, for example, through the magneto-optic effect or nonlinear processes that alter the propagation of light based on its direction. These devices can block or divert all backward-propagating modes, ensuring robust isolation regardless of the input's angular distribution.[1] In contrast, our diffractive optical designs are reciprocal systems thathaveasymmetricmodeprocessingcapabilities;thebackward light suppression achieved by our diffractive systems is effective for specific incident angles or angular ranges used during the training process. Despite being a reciprocal device, our diffractive system, with its unidirectional beam-focusing capability, can still be an effective tool in various applications, for example, freespace optical communications or laser beam shaping systems. In such cases, unidirectional diffractive optical designs can provide protection without requiring nonlinear components or magnetooptic materials. Furthermore, since our system uses isotropic diffractive layers, it can function effectively for any polarization state, offering an additional advantage over methods that are sensitive to polarization.[11,16] This polarization insensitivity, combined with its passive and compact nature, makes our approach suitable for a wide range of applications that require directional light control.

Deploying diffractive unidirectional light-focusing systems in real-world environments also presents some practical challenges, such as handling environmental noise and system misalignments, as discussed above in the experimental results. Addressing these factors would require further optimization in the design process. One potential solution is to introduce noise and misalignments intentionally during the gradient descentbased training process.[19] Furthermore, with the recent advancements in nanofabrication techniques, such as electron beam lithography[20] and two-photon polymerization,[21] the unidirectional focusing designs reported in our work can be scaled to work at other wavelength ranges, including the visible and infrared, by appropriately scaling the diffractive feature size with respect to the illumination wavelength, i.e., without the need to retrain the diffractive layers from scratch.

Although the presented designs are based on spatially coherent illumination, this framework can be extended to spatially incoherent or partially coherent input fields by leveraging the same design principles and gradient descent-based optimization methods.[22–24] For spatially incoherent or partially coherent illumination, phase-only diffractive layers can be optimized using similar unidirectional focusing-related loss functions, although simulating incoherent or partially coherent field propagation requires additional steps to statistically account for the coherence diameter at the illumination plane, which relatively increases computational demand and training time. In addition to exploring incoherent or partially coherent illumination cases, increasing the effective spectral bandwidth of unidirectional focusing systems presents another promising direction for future research. Extending these systems to operate effectively in various environments with complex, incoherent, or partially coherent light sources, as well as enhancing their robustness across broader angular ranges and spectral bandwidths, will further widen their applicability, expanding the utility of these designs for further innovations in unidirectional optical systems.

4. Experimental Section

Optical Forward Model of a Unidirectional Focusing System: In the forward model of our diffractive unidirectional focusing design, the input plane, diffractive layers, and output plane are sequentially arranged along the optical axis, with an axial spacing of d between each plane. For the numerical and experimental models, d was empirically set to 6 *mm* and 20 *mm*, respectively, corresponding to 8λ and 26.67λ, where λ = 0.75 mm is the operating wavelength. The optical forward model of a diffractive processor consists of two sequential processes: 1) free-space propagation of the light wave between consecutive planes and 2) modulation of the light wave by the apertures or the diffractive layers. The free-space propagation was modeled using the angular spectrum approach,[25] expressed as:

$$u(x, y, z + d) = \mathcal{F}^{-1}\{\mathcal{F}\{u(x, y, z)\} \cdot H(f_x, f_y; d)\} \quad (1)$$

where $u(x, y, z)$ represents the complex-valued field at a coordinate of z along the optical axis, and $u(x, y, z + d)$ is the resulting field at the coordinate of $z + d$ after propagating over an axial distance of d. Here, f_x and f_y denote the spatial frequencies along the x and y directions, respectively, while $\mathcal{F}$ and $\mathcal{F}^{-1}$ denote the 2D Fourier transform and 2D inverse Fourier transform, respectively. The free-space transfer function $H(f_x, f_y; d)$ is defined as:

$$H(f_x, f_y, d) = \begin{cases} \exp\left(jkd\sqrt{1 - \left(\frac{2\lambda f_x}{}\right)^2 - \left(\frac{2\lambda f_y}{}\right)^2}\right), & f_x^2 + f_y^2 \\ 0, & f_x^2 + f_y^2 \geq \frac{1}{\lambda^2} \end{cases} \quad (2)$$

where $j = \sqrt{-1}$ and $k = \frac{2\pi}{\lambda}$.

The diffractive layers were modeled as thin optical modulation elements. The m-th diffractive feature on k-th layer, located at (x_m, y_m, z_m), is described as:

$$t_k(x_m, y_m, z_m) = \exp\{j\phi_k(x_m, y_m, z_m)\} \quad (3)$$

where $\phi_k(x_m, y_m, z_m)$ represents the phase modulation value for the corresponding diffractive feature. During the training process, the phase values of the diffractive features are iteratively optimized to achieve the desired unidirectional beam-focusing functionality.

In the experimental demonstration, the height values of the learnable diffractive features ($h_{trainable}$) were computed based on the refractive index

of the 3D printing material.[26] Additionally, a constant substrate thickness ($h_{substrate}$ = 0.5 *mm*) was added for mechanical support of each layer.

Training Loss Function and Evaluation Metrics: In our unidirectional focusing designs, an incident plane wave is focused in one direction (A → B) while being suppressed in the opposite direction (B → A). The training loss function for the diffractive unidirectional focusing system is defined as:

$$L\left(O_{fcs}, O_{blk}, I_{fcs}, I_{blk}\right) = \square L_{EffBst}\left(O_{fcs}, I_{fcs}\right) + \square L_{EffSqz}\left(O_{blk}, I_{blk}\right) \quad (4)$$

where I_{fcs} (FOV A) and I_{blk} (FOV B) denote the input illumination in the forward and backward directions, respectively, and O_{fcs} (FOV B) and O_{blk}(FOV A) are the output fields in these directions, respectively. L_{EffBst} was used to enhance the output energy efficiency along the focusing direction (A → B) and was defined as:

$$L_{EffBst}\left(O_{fcs}, I_{fcs}\right) = \exp\left[-\square_{EffBst}\left(O_{fcs}, I_{fcs}\right)\right] \quad (5)$$

where $\square_{EffBst}(O, I)$ is the output diffraction efficiency, given by: $\square_{EffBst}$ $_{apertureB}$

$$\left|\left|\right|\right|\left|\right|_2 \quad (6)$$

$$O\left(x, y\right)^2$$

$$_{apertureA}\ I\left(x, y\right)$$

where $\sum_{(x,y)apertureA} *$ and $\sum_{(x,y)apertureB} *$ denote summation within the apertures of FOV A and FOV B, respectively.

Similarly, L_{EffSqz} was used to penalize the output diffraction efficiency in the backward direction (B → A) and was defined as:

$$L_{EffSqz}\sum\left(O_{blk}, \quad I_{FOVAblk}\right)_{FOVA}\left|\left|\right|\right|_2 \quad (7)\ O$$

$$_{apertureB}\left|I\right.$$

where $_{(x,y)} *$ represents summation across the entire FOV A. The loss weights $\square$ and $\square$ were both set to 1 to balance the two loss terms.

For the model trained to block reflections, we replaced the plane wave used as the input for the backward operation (B → A) with the output optical field resulting from the forward operation (A → B). For the model used in Figure S3 (Supporting Information), the loss weight ratio was $r = \square$ = 1. In Figure S4 (Supporting Information), we trained additional unidirectional focusing diffractive models with different loss weight ratios, $r = \square \in \{1/4, 1/3, 1/2, 1, 2, 3, 4\}$.

Regarding the multi-angle training, we used the same loss function described in Equation (5) for the forward operation, while Equation (7) was applied across all the illumination angles in the backward operation.

For the multi-wavelength diffractive unidirectional design shown in Figure 5, the loss function defined in Equation (4) was applied with equal weights across all the wavelength channels of interest.

We defined an SNR metric to evaluate the experimental results for both the forward and backward operations. Specifically, for the forward operation, the SNR was defined as:

$$SNR_{forward} = \frac{mean\left(O(x, y)_{aperture\ B}\right)}{std\left(O(x, y)_{FOV\ B-aperture\ B}\right)} \quad (8)$$

where *FOV B – aperture B* represents the region outside the aperture B but within FOV B. The *mean* and *std* calculate the average intensity and its standard deviation, respectively. As for the backward operation, the SNR was defined as:

$$\quad mean \quad x, y \quad)$$

$$SNR_{backward} = (9)\ std$$

Parameters and Digital Implementation for Numerical Analyses: Numerical analysis for the unidirectional focusing designs was performed at a wavelength of $\square$ = 0.75 mm, with the smallest sampling period matching the lateral size of the diffractive features, ˜0.53 $\square$. The circular aperture at FOV A had a diameter of 32 mm (42.67 $\square$) and it was 3.2 mm (4.3 $\square$) at FOV B. We generated customized datasets to train the diffractive unidirectional focusing systems. For normal illumination, we simulated the input using a plane wave confined within the aperture, with a uniform amplitude of 1 and a uniform phase of 0. For oblique illumination, input waves corresponding to multiple illumination angles were generated by adjusting the phase values based on the desired tilt angle, while maintaining a uniform amplitude of 1 within the aperture.

During the training process of our monochrome unidirectional focusing models, the corresponding plane wave—either at normal or oblique incidence—was propagated through the numerical optical model described above. The output was compared with the corresponding target, and the loss was calculated based on the defined loss function in Equation (4). The computed loss was backpropagated to iteratively update the phase or height values of the diffractive features of each layer. The training was conducted over 5000 iterations using the AdamW optimizer with default parameters and a learning rate of 0.001 for all models. For the multiwavelength design shown in Figure 5, plane waves of three different wavelengths were input into the model, and the above process was repeated for each wavelength.

All the diffractive unidirectional focusing models were optimized using PyTorch (v1.11.0, Meta Platforms Inc.). The training process utilized a workstation equipped with a GeForce GTX 1080Ti GPU (Nvidia Inc.), an Intel Core i7-8700 CPU (Intel Inc.), and 64 GB of RAM. Each training session for a diffractive unidirectional focusing model typically required ˜3 h.

Experimental Demonstration: The diffractive layers were fabricated using a 3D printer (Objet30 Pro, Stratasys). The apertures were also 3D printed and coated with aluminum foil to define the light-blocking regions, while the uncovered areas served as the transmission zones. A 3D-printed holder was used to assemble the diffractive layers and input objects in alignment with the positions specified in the numerical design.

A terahertz continuous-wave scanning system was used for testing our diffractive unidirectional focusing design. As depicted in Figure 7b, the

terahertz source comprised a WR2.2 modular amplifier/multiplier chain (AMC) with a compatible diagonal horn antenna (Virginia Diodes Inc.). The AMC received a 10-dBm radiofrequency (RF) input signal at 11.1111 GHz (f_{RF1}), which was multiplied 36 times to generate output radiation at 400 GHz, corresponding to a wavelength of □ = 0.75 mm. The AMC output was modulated with a 1-kHz square wave for lock-in detection. The assembled diffractive unidirectional focusing system was positioned ˜600 mm from the horn antenna's exit aperture, ensuring a nearuniform plane wave illumination across its input field of view (FOV A), with dimensions of 36 × 36 mm^2 (i.e., 48□ × 48□). The intensity distribution within the output FOV (B) of the imager was scanned with a step size of 0.8 mm using a single-pixel detector system. The detector comprised a mixer/AMC (Virginia Diodes Inc.) mounted on an *xy*-positioning stage, assembled from two linear motorized stages (Thorlabs NRT100). The detector also received a 10-dBm sinusoidal local oscillator signal at 11.083 GHz (f_{RF2}) for mixing to down-convert the output signal to 1 GHz.

The down-converted 1-GHz signal was amplified by a low-noise amplifier (Mini-Circuits ZRL-1150-LN+) with an 80-dBm gain, and filtered through a 1-GHz band-pass filter (±10 MHz) (KL Electronics 3C40-1000/T10-O/O)

to suppress noise from unwanted frequency bands. A tunable attenuator (HP 8495B) was then used for linear calibration, and the processed signal was sent to a low-noise power detector (Mini-Circuits ZX47-60). The detector output voltage was measured by a lock-in amplifier (Stanford Research SR830) using the 1-kHz square wave as a reference. The lock-in readings were subsequently calibrated to a linear scale.

Supporting Information

Supporting Information is available from the Wiley Online Library or from the author.

Acknowledgements

The authors acknowledge the support of NSF (Grant # 2401393).

Conflict of Interest

The authors have a pending patent application on unidirectional diffractive processors.

Data Availability Statement

The data that support the findings of this study are available from the corresponding author upon reasonable request.

Keywords

diffractive optics, reciprocal optical systems, unidirectional focusing

Received: December 9, 2024
Revised: February 28, 2025
Published online: March 20, 2025

[1] D. Jalas, A. Petrov, M. Eich, W. Freude, S. Fan, Z. Yu, R. Baets, M. Popovi´c, A. Melloni, J. D. Joannopoulos, *Nat. Photonics* **2013**, *7*, 579. [2] M. Fang, F. Shi, Y. Chen, *Plasmonics* **2016**, *11*, 197.
[3] Z. Lin, H. Ramezani, T. Eichelkraut, T. Kottos, H. Cao, D. N. Christodoulides, *Phys. Rev. Lett.* **2011**, *106*, 213901.
[4] H. Lee, *Appl. Opt.* **1987**, *26*, 969.
[5] Z. Wang, S. Fan, *Opt. Lett.* **2005**, *30*, 1989.
[6] L. Bi, J. Hu, P. Jiang, D. H. Kim, G. F. Dionne, L. C. Kimerling, C. A. Ross, *Nat. Photon* **2011**, *5*, 758.
[7] Y. Shoji, M. Ito, Y. Shirato, T. Mizumoto, *Opt. Express* **2012**, *20*, 18440.
[8] C. G. Poulton, R. Pant, A. Byrnes, S. Fan, M. J. Steel, B. J. Eggleton, *Opt. Express* **2012**, *20*, 21235.
[9] M. Krause, H. Renner, E. Brinkmeyer, *Electron. Lett.* **2008**, *44*, 691.
[10] K. Gallo, G. Assanto, K. R. Parameswaran, M. M. Fejer, *Appl. Phys. Lett.* **2001**, *79*, 314.
[11] M. J. Lockyear, A. P. Hibbins, K. R. White, J. R. Sambles, *Phys. Rev. E* **2006**, *74*, 056611.
[12] A. E. Serebryannikov, *Phys. Rev. B* **2009**, *80*, 155117.
[13] J. Xu, X. Zhuang, P. Guo, W. Huang, W. Hu, Q. Zhang, Q. Wan, X. Zhu, Z. Yang, L. Tong, *Sci. Rep.* **2012**, *2*, 820.
[14] D. L. Sounas, A. Alù, *Nat. Photonics* **2017**, *11*, 774.
[15] B. Yao, X. Zang, Z. Li, L. Chen, J. Xie, Y. Zhu, S. Zhuang, *Photon. Res.* **2020**, *8*, 830.
[16] A. R. Davoyan, A. M. Mahmoud, N. Engheta, *Opt. Express* **2013**, *21*, 3279.
[17] A. M. Mahmoud, A. R. Davoyan, N. Engheta, *Nat. Commun.* **2015**, *6*, 8359.
[18] C. Menzel, C. Helgert, C. Rockstuhl, E.-B. Kley, A. Tünnermann, T. Pertsch, F. Lederer, *Phys. Rev. Lett.* **2010**, *104*, 253902.
[19] D. Mengu, Y. Zhao, N. T. Yardimci, Y. Rivenson, M. Jarrahi, A. Ozcan, *Nanophotonics* **2020**, *9*, 4207.
[20] Y. Chen, *Microelectron. Eng.* **2015**, *135*, 57.
[21] S. O'Halloran, A. Pandit, A. Heise, A. Kellett, *Adv. Sci.* **2023**, *10*, 2204072.
[22] G. Ma, C.-Y. Shen, J. Li, L. Huang, Ç. I¸sıl, F. O. Ardic, X. Yang, Y. Li, Y. Wang, M. S. S. Rahman, A. Ozcan, *APN* **2024**, *3*, 066008.
[23] M. S. S. Rahman, X. Yang, J. Li, B. Bai, A. Ozcan, *Light Sci Appl* **2023**, *12*, 195.
[24] X. Yang, M. S. S. Rahman, B. Bai, J. Li, A. Ozcan, *APN* **2024**, *3*, 016010. [25] X. Lin, Y. Rivenson, N. T. Yardimci, M. Veli, Y. Luo, M. Jarrahi, A. Ozcan, *Science* **2018**, *361*, 1004.
[26] Y. Luo, D. Mengu, N. T. Yardimci, Y. Rivenson, M. Veli, M. Jarrahi, A. Ozcan, *Light Sci. Appl.* **2019**, *8*, 112.